Fabrication and Characterization of $Gd_2O_2SO_4:Tb^{3+}$ Phosphors by Sol-gel Method

I. Aritman[1,*], S. Yildirim[1], A. Kisa[1], L. F. Guleryuz[2], M. Yurddaskal[1], T. Dikici[1] and E. Celik[1]

[1]*Dokuz Eylul University, Production and Application Center of Electronic Materials (EMUM), Faculty of Engineering, Buca Main Campus, Izmir, Turkey*
[2]*Ege University, Department of Mechanical Engineering, Bornova, Izmir, Turkey*
[*]*Corresponding author: idil.aritman@deu.edu.tr*

Abstract. The objective of the innovative approaches of the scintillation materials to be used in the digital portal imaging systems in the radiotherapy applications is to research the GOS material production that has been activated with the rare earth elements (RE), to produce the scintillation detectors that have a rapid imaging process with a lesser radiation and higher image quality from these materials and to apply the radiographic imaging systems. The GOS: Tb^{3+} showed high emission peak and high x-ray absorption properties which have been determined for application to mammography and dental radiography. In this study, $Gd_2O_2SO_4:Tb^{3+}$ phosphors were fabricated by the sol-gel method that is a unique technique and not previously applied. Besides, the structural characterization of GOS: Tb^{3+} has been investigated. The strongest emission peak located at 549 nm under 312 nm UV light excitation was appeared on the GOS: Tb^{3+} phosphor particles. The characterization processing optimized by using FTIR, DTA-TG, XRD, XPS, SEM and the luminescence spectroscopy.

Keywords: Radiography imaging; GOS phosphors; Sol-gel.
PACS: 78.55.Kz, 81.05.Bx, 81.20.Fz.

INTRODUCTION

Scintillators have induced intensive interest within research in the last few years, due to their technological importance and imaging application [1-3]. During the last half-century, there has been rapid development in the field of X rays-visible emission scintillator [4-6]. Scintillation materials have been used in digital radiographic imaging systems with the help of the developing technology in the recent years [7]. These materials are continuously being improved because of the demand. Gadolinium oxysulfate ($Gd_2O_2SO_4$) has quite interesting and unusual magnetic properties at low temperature [8, 9]. $Gd_2O_2SO_4$ (GOS) indicates favorable properties such as the high luminescence efficiency, the color purity and the long emission lifetime values [10-13]. Rare Earth doped GOS scintillator materials with unique optical and chemical properties make them important in digital imaging and phosphor screens. For these reasons, GOS is a good scintillation material which transforms the ultraviolet or X rays into the visible light in the digital imaging systems [14].

In the literature, $Gd_2O_2SO_4:Tb^{3+}$ nanopieces were synthesized by a combined approach of electrospinning and calcination at 1000 ^oC in mixed gas of sulfurdioxide

Proceedings of the 6th International Advances in Applied Physics and Materials Science Congress & Exhibition
AIP Conf. Proc. 1809, 020003-1–020003-8; doi: 10.1063/1.4975418
Published by AIP Publishing. 978-0-7354-1477-8/$30.00

and air [15]. In another study, gadolinium dodecyl sulphate was synthesized by reacting stoichiometric amount of starting materials. Further, gadolinium sulphate $Gd_2(SO_4)_3$, and gadolinium oxysulfate $Gd_2O_2SO_4$ were obtained by decomposing the gadolinium dodecyl sulphate complex in air atmosphere. The obtained GOS: Eu^{3+} nanophosphors were collected for further characterization and were examined the effect of temperature on the structural and optical properties of GOS: Eu^{3+} nanophosphors [16]. Also, pure $(Gd_{1_x}, Eu_x)_2O_2SO_4$ nanophosphors were synthesized with commercially available the starting materials by a novel co-precipitation method [17]. In this study, characteristic properties of GOS:Tb^{3+} scintillation material fabricated by the distinctive sol-gel method has been investigated via the DTA/TG, FTIR, XRD, SEM, XPS and PL spectra device.

EXPERIMENTAL DETAILS

Production of GOS nanoparticles was carried out by the sol-gel method. First of all, starting materials composed of Gadolinium (III) Acetate Hydrate ($Gd(CH_3CO_2).xH_2O$), Urea ($CO(NH_2)_2$), Ammonium sulfate ($(NH_4)_2SO_4$) and Terbium (III) nitrate pentahydrate ($Tb(NO_3)_3.5H_2O$) were weighed out and then the solution was prepared using the pure water. The amount of Tb dopant was %0.01 mole. The prepared solution was stirred until it became transparent in an ultrasonic mixer at 80°C in order to facilitate the dissolution of the powder based precursor chemicals. The sol-gel is an advanced materials production method, with a very wide spectrum of gel, polymeric crystalline and glassy phases which are generally in liquid form. For these reasons, if the starting point in the liquid form is prepared carefully, the final structure will be successful in the sol-gel method. Various tests were applied for the characterization of the prepared solution within this context. A blur test of solution was performed using standard VELP TB1 Model turbidity meter. The pH value was measured by the standard pH meter with the help of the Mettler Toledo Electrode.

Differential Thermal Analysis / Thermogravimetric (DTA / TG) and Fourier Transform Infrared (FTIR) analyses of synthesized xerogel powder were performed. SHIMADZU scanning DTA / TGA was used. The produced solution was dried at 200°C, and then powders were obtained. The prepared xerogel powders were analyzed between 25°C – 1000°C temperatures with 10°C/min. heating rate in an oxygen atmosphere.

Depending on increasing temperatures, FTIR analyzes of liquid, gel and calcined powders at 950°C were conducted in order to determine how it changed the bond structures in transition to final ceramic structure from liquid form. The wave number range of the absorption spectrum between 4000 and 400 cm^{-1} was obtained by FTIR (Thermo Scientific NICOLET IS10) device. The production of scintillator material was obtained at 950°C.

The microstructural properties of the produced scintillator materials have been identified. The detection of the current phase of produced GOS:Tb^{3+} based material was analyzed using the Thermo Scientific Cu-Kα model X-ray diffraction (XRD). The Scanning Electron Microscope (SEM) device was utilized to determine the microstructures and surface characteristics of the GOS:Tb^{3+} material. The elemental

analysis of GOS:Tb^{3+} was performed using the Thermo-Scientific Cu-Kα model X-ray Photoelectron Spectroscopy (XPS). The excitation and emission values of GOS:Tb^{3+} were analyzed using the PL Spectra.

RESULTS and DISCUSSION

Fig.1 shows the XRD pattern of the $Gd_2O_2SO_4$:Tb^{3+} nanoparticles annealed at 950°C. Shown in Fig. Y, it is clear that all of these peaks can be indexed to $Gd_2O_2SO_4$ according to JCPDS Card no.29-0613. The obtained diffraction pattern is consistent with the data reported in literature and no other impurity phases can be observed [16-18]. The crystal structure of $Gd_2O_2SO_4$ can be described by an alternating stacking of sulfate (SO_4^{2-}) and $Gd_2O_2^{2+}$ layers along the a-axis. The $Gd_2O_2^{2+}$ layer consists of GdO_4 tetrahedra linked together by edge sharing. The lattice parameters were calculated using the XRD pattern, a=4.04 Å, b= 4.17 Å, c= 12.97 Å. The similarity of peak broadening and similar radius of doping elements ($r_{(Gd^{3+})}$=0.0938 nm, $r_{(Tb^{3+})}$=0.095 nm) in the entire diffraction pattern indicates that there were no vast changes in crystallite size.

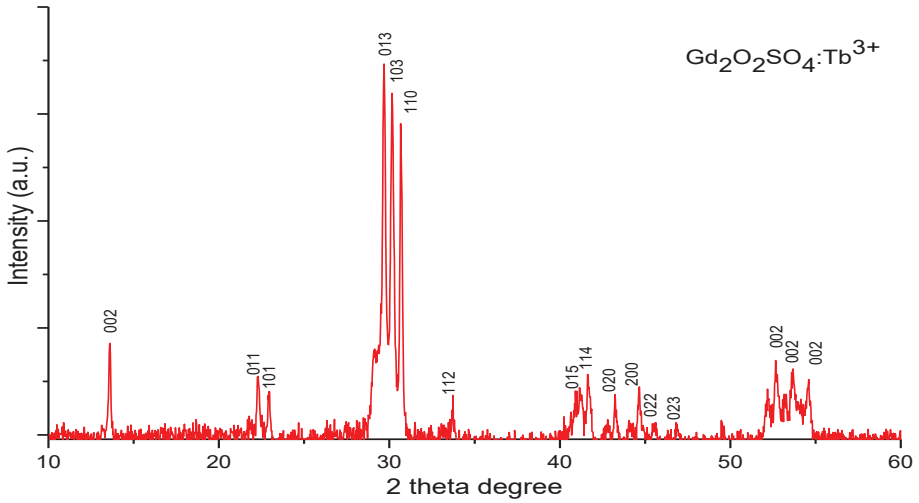


Figure 1. XRD pattern of produced GOS: Tb^{3+} particles annealed at 950°C.

The FTIR spectrum of respectively sol, gel and produced particles at 950°C of GOS: Tb^{3+} has been given in Fig.2. Peaks at <650 cm^{-1} on spectrum of produced sample at 950°C indicated the presence of the sulfuric acid in the structure. Peaks at 670-570 cm^{-1} and peak at 526 cm^{-1} showed respectively the Gd-S bonds and vibrations on the Gd-O bonds. The symmetric stretching vibrations in 1070-1030 cm^{-1} and 1160-1140 cm^{-1} represented bonds in the sulfur structure. The observed multiple peaks between 1200-1050 cm^{-1} were owned by the S = O stretching vibration (asymmetric stretching vibrations) [19].

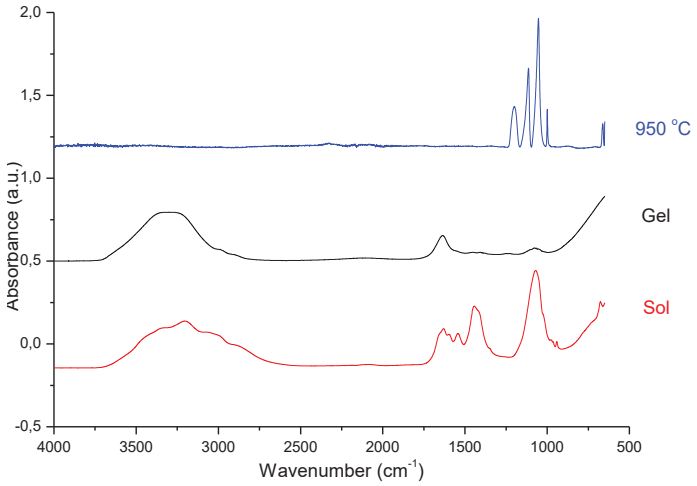


Figure 2. FTIR graphics of sol, gel and produced particles at 950°C of GOS:Tb^{3+} .

Peaks at 3750-3000 cm^{-1} and peak at 1620 cm^{-1} indicated the H-OH bond vibrations in the structure. The observed multiple peaks at 1600-1400 cm^{-1} pointed C = C and C = O bonds in the aromatic structure which were absorbed onto the sample stages of the decomposition. Peaks at 1200-1000 cm^{-1} represented the presence of ether (R-O-R) in the structure. Peaks at 1000-750 cm^{-1} were observed due to the hydrogen bonded π bound carbons (=C-H) [20].

The TG-DTA chart of GOS: Tb^{3+} gel sample produced by the sol-gel method is seen in Figure 3. DTA-TG curves were found at starting from the room temperatures to 950°C.

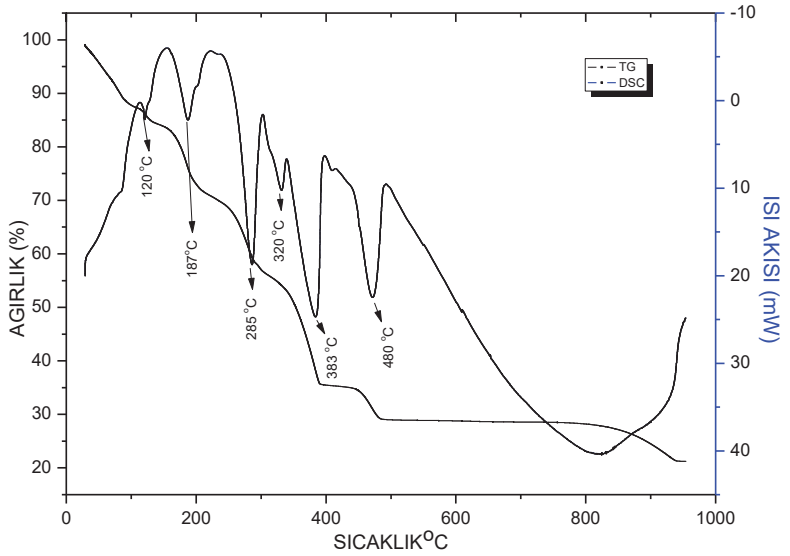


Figure 3. DTA/TG curves of GOS:Tb^{3+} particles.

The TG curve showed a continuous decrease from the room temperature to the final temperature (See Fig.3). There were two major endothermic peaks which led to the loss of mass on the TG curve. These were physical and chemical water at 22-250 ^{o}C and loss of CO_2, CO_3^{2-} anions because of the chemical reactions moving away from structure [21].

The formed peaks at around 200°C with the increasing temperature on the DTA curve were chemical reactions which showed sulfur separated from other compounds, because the melting temperature of sulfur is known to be 119.3°C [22]. There were no endothermic reaction from 480°C and it was not serious weight loss up to 950°C.

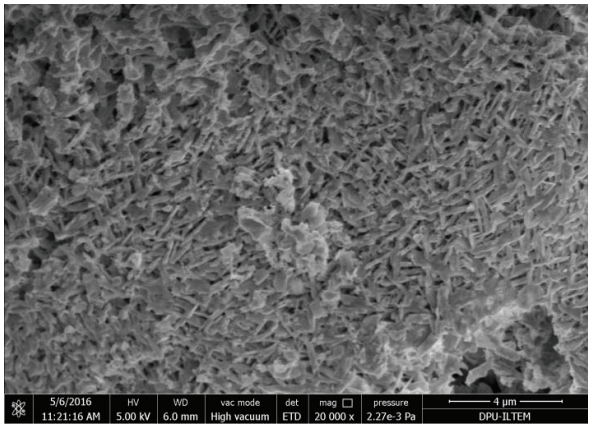


Figure 4. SEM image of GOS:Tb^{3+} nanoparticles (20x).

The SEM image of GOS: Tb^{3+} nanoparticles at 20000 magnifications are shown in Fig.4. The SEM image clearly indicated that GOS: Tb^{3+} structure consisted of cactus needle-like nanoparticles assembled by orientation mechanism. Each needle grains were observed to be 100-200 nm in size. These results showed that the rod-like structure was more stable than the spherical structure.

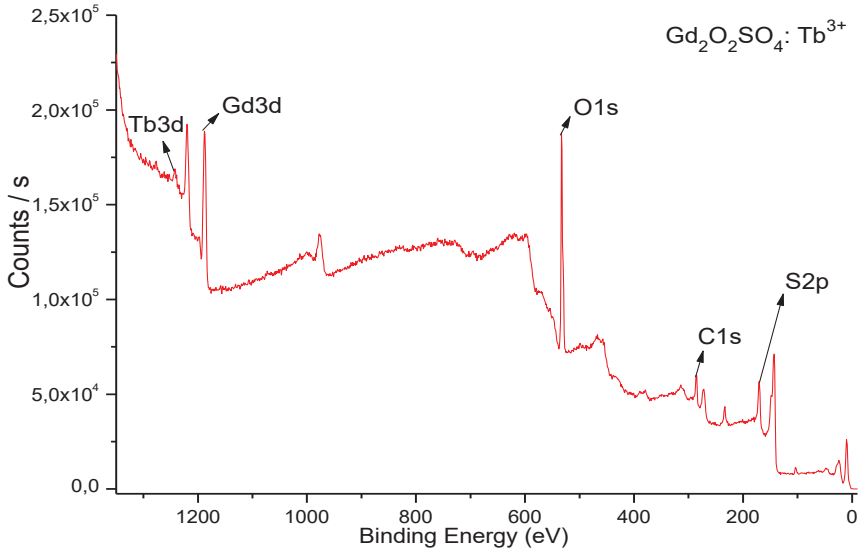


Figure 5. XPS pattern of GOS:Tb^{3+} powders.

The surface composition of GOS: Tb^{3+} nanophosphor was further analyzed by XPS measurements. As demonstrated in Fig. 5, the elements of Gd, O, S, C and Tb can be detected. The carbon on the surface of GOS: Tb^{3+} nanophosphor is ascribed to the adsorbed CO_2 from the ambient environment and the adventitious hydrocarbon from the XPS instrument itself [23].

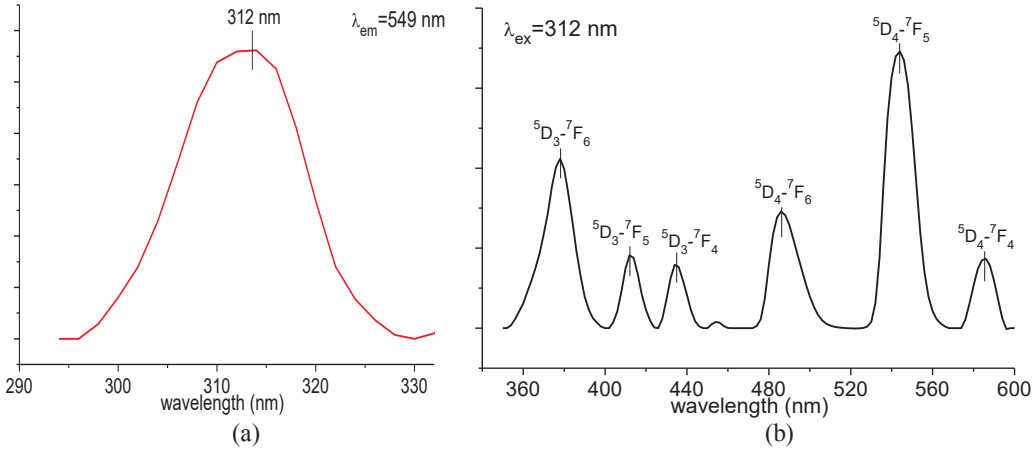


Figure 6. a) Excitation spectra of the GOS:Tb^{3+}; b) Emission spectra of the GOS:Tb^{3+} .

The excitation and emission spectra were recorded at room temperature for the GOS: Tb^{3+} powders which were synthesized via the sol-gel method. Typical results were illustrated in Fig. 6 a and b. The excitation spectra of GOS:Tb^{3+} phosphor investigated at 549 nm emission was measured in the range of 290-330 nm as it was shown in Fig. 2 a. This reveals a strong band around 312 nm. The excitation peak in band at 312 nm originates from the transitions of $^8S_{7/2}$ - $^6P_{7/2}$ of Gd^{3+}. This stronger excitation peak based on the intratransition of Gd^{3+} in GOS:Tb^{3+} nanophosphor

indicates that an efficient energy transfers from Gd^{3+} to Tb^{3+} in GOS:Tb^{3+} nanophosphor [24].

CONCLUSION

100-200 nm in size and cactus needle-like GOS: Tb^{3+} phosphor particles were synthesized by the sol-gel method. The effects of Gd^{3+} ions on the luminescence behavior of nanoparticles are analyzed. The content of Tb rare earth dopant in nanoparticles is examined. Powders were characterized by XRD, FTIR, DTA/TG, SEM, XPS and PL Spectra devices. The nanoparticles excited by a 322 nm light showed luminescence behavior with the strongest emission peak at 549 nm due to the $^5D_4 \rightarrow {}^7F_5$ transition of Tb^{3+}. In the case, the sol-gel method is suitable for producing pure GOS: Tb^{3+} nanoparticles.

ACKNOWLEDGEMENTS

Center for Production and Applications of Electronic Materials (EMUM) where this research was carried out.

REFERENCES

1. C. W. Van Eijk, *Physics in medicine and biology*, **47** (8), R85 (2002).

2. T. Yanagida, N. Kawaguchi, Y. Fujimoto, K. Fukuda, Y. Yokota, A. Yamazaki, A. Yoshikawa, *Optical Materials*, **33** (8), 1243-1247 (2011).

3. M. Nikl, *Measurement Science and Technology*, **17**(4), R37 (2006).

4. S. Yildirim, M. Yurddaskal, T. Dikici, I. Aritman, K. Ertekin, E. Celik, *Ceramics International*, **42** (9), 10579-10586 (2016).

5. A. Garcıa-Murillo, C. Le Luyer, C. Dujardin, T. Martin, C. Garapon, C. Pedrini, J. Mugnier, *Nuclear Instruments and Methods in Physics Research Section A: Accelerators, Spectrometers, Detectors and Associated Equipment*, **486** (1), 181-185 (2002).

6. J. Touš, M. Horvath, L. Pina, K. Blažek, B. Sopko, *Nuclear Instruments and Methods in Physics Research Section A: Accelerators, Spectrometers, Detectors and Associated Equipment*, **591** (1), 264-267 (2008).

7. J. Touš, M. Horvath, L. Pina, K. Blažek, B. Sopko, *Nuclear Instruments and Methods in Physics Research Section A: Accelerators, Spectrometers, Detectors and Associated Equipment*, **591** (1), 264-267. (2008).

8. W. Paul, *Journal of Magnetism and Magnetic Materials*, **87** (1-2), 29-37 (1990).

9. G. Wang, Q. Peng, Y. Li, *Accounts of Chemical Research*, **44** (5), 322-332 (2011).

10. S. W. Kim, T. Masui, N. Imanaka, *Electrochemistry*, **77** (8), 611-613 (2009).

11. J. B. Lian, B. X. Wang, X. D. Li, X. D. Sun, *Journal of Functional Materials*, **12**, 015 (2010).

12. J. Lian, J. Wu, X. Li, X. Sun, *Materials Review*, **20**, 029 (2010).

13. J. B. Lian, X. D. Li, S. F. Ding, T. Gao, X. D. Sun, *Journal of Functional Materials*, **7**, 008 (2008).

14. J. B. Lian, W. G. Wang, B. X. Wang, J. Li, In *Advanced Materials Research*, **299**, 612-615 (2011).

15. R. Manigandan, K. Giribabu, R. Suresh, S. Munusamy, S. Muthamizh, T. Dhanasekaran, V. Narayanan, *RSC Advances*, **5** (10), 7515-7521. (2015).

16. L. Song, P. Du, Q. Jiang, H. Cao, J. Xiong, *Journal of Luminescence*, **150**, 50-54 (2014).

17. J. Lian, X. Sun, Z. Liu, J. Yu, X. Li, *Materials Research Bulletin*, **44** (9), 1822-1827 (2009).

18. H. Guo, N. Dong, M. Yin, W. Zhang, L. Lou, S. Xia, *The Journal of Physical Chemistry B*, **108** (50), 19205-19209 (2004).

19. M. Xing, W. Cao, T. Pang, X. Ling, N. Chen, *Chinese Science Bulletin*, **54** (17), 2982-2986 (2009).

20. L. Hernández-Adame, F. Medellín-Rodríguez, A. Méndez-Blas, R. Vega-Acosta, G. Palestino, *International Society for Optics and Photonics (In SPIE OPTO)*, 86261P-86261P (2013).

21. S. Som, A. Choubey, S. K. Sharma, *Journal of Experimental Nanoscience*, **10** (5), 350-370 (2015).

22. A. Ubaldini, C. Artini, G. Costa, M. Carnasciali, R. Masini, *Journal of Thermal Analysis and Calorimetry*, **84** (1), 207-211 (2006).

23. Y. Tian, W. H. Cao, X. X. Luo, Y. Fu, *Journal of Alloys and Compounds*, **433** (1), 313-317 (2007).

24. F. Wang, D. Liu, B. Yang, Y. Dai, *Vacuum*, **87**, 55-59. (2013).